CHEMISTRY OF MATERIALS

ARTICLE

pubs.acs.org/cm

Thallium Chalcogenide-Based Wide-Band-Gap Semiconductors: $TlGaSe_2$ for Radiation Detectors

Simon Johnsen,[†] Zhifu Liu,[‡] John A. Peters,[‡] Jung-Hwan Song,[§] Sebastian C. Peter,[†] Christos D. Malliakas,[†] Nam Ki Cho,[‡] Hosub Jin,[§] Arthur J. Freeman,[§] Bruce W. Wessels,[‡] and Mercouri G. Kanatzidis*[,†]

[†]Department of Chemistry, [‡]Department of Materials Science and Engineering, Materials Research Center, and [§]Department of Physics and Astronomy, Northwestern University, Evanston, Illinois 60208, United States

Supporting Information

ABSTRACT: The wide-band-gap semiconductor thallium gallium selenide ($TlGaSe_2$) is promising for X-ray and γ-ray detection. In this study, the synthesis and crystal growth of semiconducting $TlGaSe_2$ was accomplished using a stoichiometric combination of TlSe, Ga, and Se and a modified Bridgman method. These large detector-grade crystals can be synthesized and cut to dimensions appropriate for a detector. The crystals have mirror-like cleaved surfaces and are transparent red, in agreement with a band gap of 1.95 eV observed in absorption measurements. Single-crystal X-ray diffraction refinements confirm that $TlGaSe_2$ crystallizes in the monoclinic $C2/c$ space group with a layered crystal structure consisting of planes of $GaSe_4$ corner-sharing tetrahedra connected by weak Tl−Se bonds. Electronic band structure calculations made using the full-potential linearized augmented plane wave method with the screened-exchange local density approximation, including spin orbit coupling, indicate the unusual characteristic of the hole effective mass being lower than that of the electrons. Photoconductivity measurements on the grown $TlGaSe_2$ crystals show mobility−lifetime ($\mu\tau$) products of electrons and holes approaching the values of the state-of-the-art commercial material $Cd_{0.9}Zn_{0.1}Te$. The promising properties of this material system are confirmed by the ability of a $TlGaSe_2$-based detector to show good signal response to X-rays and resolve Ag K radiation energetically.

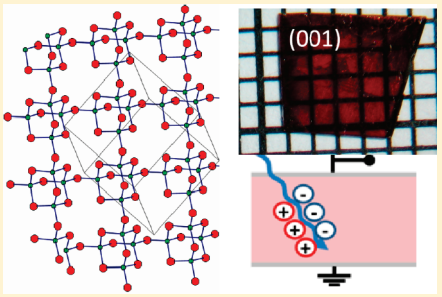

KEYWORDS: $TlGaSe_2$, radiation detector, crystal growth, photoconductivity, chalcogenide, gamma-ray detector, semiconductor, crystal growth

INTRODUCTION

Wide-band-gap semiconductors with high mass densities are attracting strong interest as X-ray and γ-ray detectors in biomedical imaging, spectroscopic instrumentation, security applications, and for several scientific purposes, because they offer the possibility of higher energy resolution than presently used technologies, such as scintillation detectors.[1−5] Currently, $Cd_{0.9}Zn_{0.1}Te$ (CZT) is the preferred material for X-ray and γ-ray detection in semiconductor devices operating at room temperature.[2,6] However, several problems are associated with the synthesis of detector-grade CZT, as the material is prone to form macroscopic defects, such as grains, cracks, and tellurium precipitates, which, in combination with poor intrinsic hole mobility, give limited device resolution.[2,6,7] Because of these issues, new superior detector-grade materials are desirable. Appropriate materials are highly dense, wide-band-gap semiconductors (>1.5 eV) with high average Z value, high electrical resistivity, and high mobility-lifetime products ($\mu\tau$) of the charge carriers.[1,2,4] The value of $\mu\tau$ for electrons and holes should be as high as possible, because it amounts to a figure of merit. Efforts on alternative materials are mainly focused on heavy-metal halides (e.g., HgI_2, TlBr, and $TlBr_{1-x}I_x$, PbI_2, and BiI_3).[3−5] Materials chemists have had little impact in this area thus far, but there is significant potential in designing new compounds to match the specific property requirements.

Because solid-state metal chalcogenides show a broad diversity of semiconducting properties (e.g., a wide range of accessible and tunable energy band gaps) and can be prepared in complex stoichoimetries and crystal structures, they present a promising source of materials for the detection of hard radiation. Particularly interesting are thallium-containing metal chalcogenides, because of the high mass density that can be attained, which, in turn, increases the absorption coefficient of the materials for γ-rays. Here, we focused on $TlGaSe_2$ as a promising candidate in a new class of materials for X-ray detection. $TlGaSe_2$ has been studied extensively, because of its dielectric properties, which are related to two phase transitions (at 107 and 120 K); interested readers are referred to reviews on the subject given in refs 8 and 9. At room temperature, $TlGaSe_2$ crystallizes in the monoclinic $C2/c$ $KInS_2$ structure[10,11] with the unit cell shown in Figure 1, where a = 10.77 Å, b = 10.77 Å, c = 15.63 Å, and β = 100.06°.[8,10,11] $TlGaSe_2$ forms red crystals with a reported indirect band gap of 1.93 eV, although there is some controversy about this (to be discussed later).[12] The high-Z-value element thallium (Z = 81) gives this compound a high density of 6.4 g cm^{-3} and good X-ray and γ-ray stopping power. Figure 2 shows the attenuation lengths

Received: April 2, 2011
Revised: May 2, 2011
Published: May 31, 2011

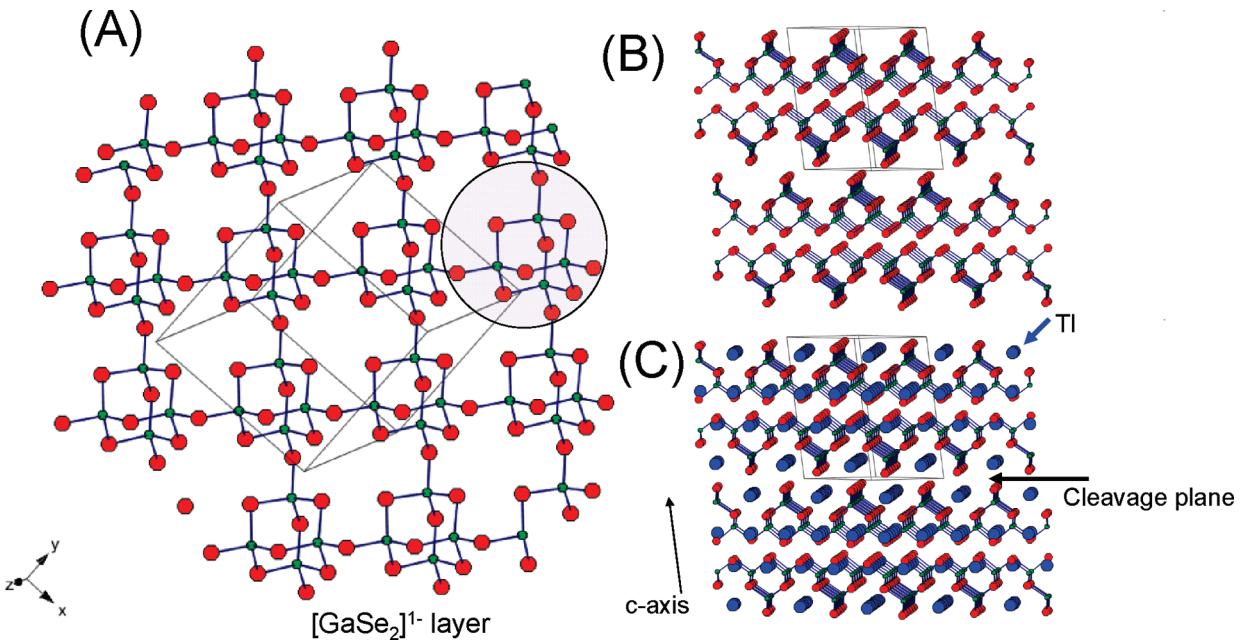

Figure 1. (A) The infinite $[GaSe_2]^-$ layer composed of corner-sharing $[Ga_4Se_{10}]$ adamantine clusters. Shaded circle indicates a single cluster. (B) Stacking of $[GaSe_2]^-$ layers, with Tl atoms removed for clarity. (C) Unit cell of $TlGaSe_2$ at 293 K, as seen along the *b*-axis.

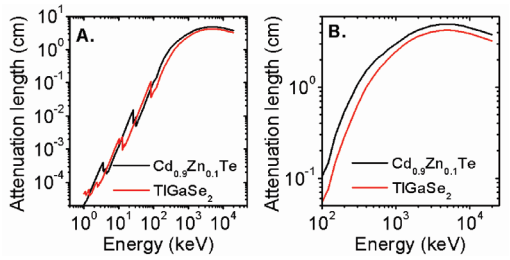

Figure 2. (A) Calculated attenuation length, as a function of the incident photon energy in $TlGaSe_2$ and CZT. (B) Expanded view of the high-energy region.

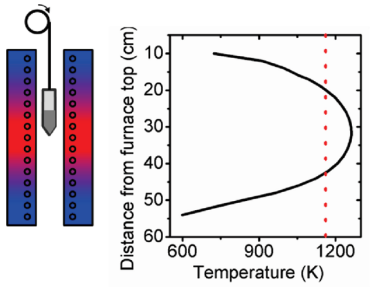

Figure 3. Schematic of the Bridgman furnace setup and measured temperature profile along its length.

of CZT and $TlGaSe_2$, which were calculated using the approach described by Seltzer from the atomic attenuation coefficients,[13] and are in agreement with literature values.[14] The stopping power of $TlGaSe_2$ is significantly greater than that of CZT in most of the depicted energy range, especially at high incident photon energies. As an example, for the 662 keV radiation of ^{137}Cs, the attenuation length of CZT is 2.3 cm and only 1.7 cm for $TlGaSe_2$. The high attenuation coefficient implies that the requirements for the $\mu\tau$ product can be relaxed somewhat, since the distance that the charge carriers must diffuse to the electrodes for detection is less than that in CZT. Because of these attributes, $TlGaSe_2$ is now starting to attract attention as a detector material.[15,16] However, neither $\mu\tau$ products nor pulse height spectra have been reported, and Kahler et al.[17] did not find any X-ray conductivity response to Cu Kα irradiation.

The present study explores a ternary member of a promising class of wide-band-gap semiconductors for X-ray and γ-ray detection: thallium chalcogenides. Here, we describe the synthesis, crystal growth, and characterization of $TlGaSe_2$. Large, high-purity single crystals have been grown and cut to detector-size dimensions. We report the electrical and photoelectrical properties of these crystals, with a focus on relevant detector material quantities. We find that the synthesized $TlGaSe_2$ crystals have resistivities in the appropriate range and high $\mu\tau$ values, approaching that of commercial CZT, which is regarded as the benchmark material for room-temperature applications. This is a highly promising development and points to the chalcogenide family as a potentially rich source of detector materials. Detailed first-principles electronic band structure calculations show little anisotropy and high dispersion of both conduction and valence bands, which suggests good transport properties of both carrier types (e.g., electrons and holes) along all crystal directions. Finally, we demonstrate that a detector device made from $TlGaSe_2$ crystals can detect hard X-rays from a Ag X-ray tube and resolve the Ag K peak energetically.

EXPERIMENTAL SECTION

$TlGaSe_2$ was synthesized using TlSe and elemental gallium and selenium as starting materials. TlSe, which melts congruently at 350 °C,[17] was made from elemental thallium (99.99% metal basis, Alfa Aesar) and selenium (99.999% metal basis, Tellurex, Inc.). The stoichiometric mixture was reacted at 500 °C and subsequently grown via the Bridgman method in a single-zone furnace kept at 450 °C, using the thermal profile of the furnace to provide the appropriate conditions for

dx.doi.org/10.1021/cm200946y |*Chem. Mater.* 2011, 23, 3120–3128

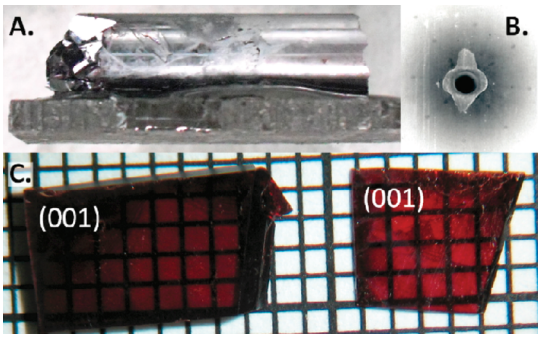

Figure 4. (A) A $TlGaSe_2$ single-crystal sample grown using the Bridgman method. The sample is mounted for cutting on a graphite substrate using Crystalbond. (B) Typical Laue X-ray back-reflection pattern from a crystal cleaved parallel to the *ab* plane. (C) Typical crystals cut and cleaved from the Bridgman sample shown in panel A.

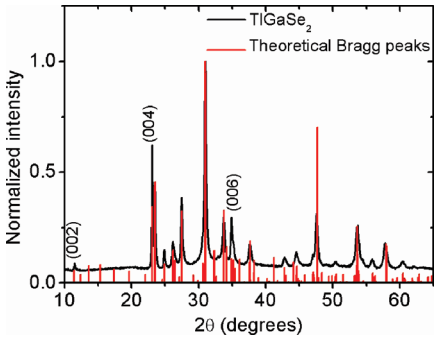

Figure 5. Powder X-ray diffraction (XRD) pattern for ground $TlGaSe_2$ crystals (Cu Kα radiation). Theoretical Bragg peaks calculated from the single-crystal refinement are shown.

crystallization. In atmospheric air, a thin oxide layer forms on Ga. In order to avoid oxide contamination, Ga was melted to move the lighter oxide film to the surface of the melt. Using a plastic syringe (plastic was used, since gallium readily dissolves many metals, even at low temperature), gallium without oxide contaminants can be extracted (see the Supporting Information). TlSe, gallium, and selenium were then mixed in stoichiometric ratio in a glovebox under a N_2 protective atmosphere with O_2 and H_2O levels below 0.1 ppm. The starting materials were sealed in a quartz tube under a 10^{-4} mbar vacuum and, in a separate step, reacted at 950 °C before a vertical Bridgman growth was initiated with the temperature gradient and furnace setup shown in Figure 3. The pulling speed was 0.7 mm h^{-1}. Using a Struers Accutom-50 waferizing saw equipped with a 300-μm-wide diamond-impregnated blade, the Bridgman samples were cut into segments from which red transparent single crystals were cleaved with mirror-like surfaces (Figure 4C). The quality of the synthesized wafers was checked using transmitted polarized light. The crystals were oriented using Laue X-ray back-reflection that was recorded on an image plate in a home-built setup equipped with a silver target X-ray tube. The scanned X-ray diffraction (XRD) image was oriented using the software OrientExpress.[18]

In order to optimize the crystal growth conditions, differential thermal analysis (DTA) was performed on a computer-controlled Shimadzu Model DTA-50 thermal analyzer. The sample shows a melting endotherm with an onset at 815 °C and a crystallization exotherm with a peak at 781 °C. The heating rate was 5 K min^{-1}. Powder XRD was recorded on a CPS 120 Inel equipped with Cu Kα radiation. DC conductivity was measured using a Keithley Model 617 electrometer. Previous publications have reported that conducting silver paste and indium can create ohmic contacts to $TlGaSe_2$.[19−21] In the present work, ohmic contacts were not observed, despite several attempts with various contact materials and solders. Conducting silver paste, indium, Pb−Sn solder, Tl_3Se_7 eutectic, and sputtered Ti/Au contacts were among the attempted contact materials, and we found sputtered Ti/Au contacts to be superior. The enclosure of the resistivity adapter shields the sample from electromagnetic interference and eliminates illumination of the sample and, hence, any photoconductive response.

The optical transmission spectrum was measured on a Lambda 1050 UV−vis−IR spectrophotometer in the range of 300−1500 nm. Photoconductivity was measured in a custom setup. The sample was illuminated with a chopped He−Ne laser (633 nm). The sample time-dependent photocurrent was recorded as a function of positive and negative bias voltages of up to 250 V. The chopper frequency was kept at 51 Hz, and the load resistance was maintained at 5.02 kiloohm (kΩ).

Photoluminescence was measured on a (001)-oriented $TlGaSe_2$ crystal. The sample is illuminated by a chopped 325-nm line from a He−Cd laser. The photoluminescence signal is dispersed by a 0.75-m SPEX grating monochromator and detected by a Hamamatsu Model R928 photomultiplier tube and a photon-counting system coupled to the preamplifier linked to the chopper frequency.

Detector properties were probed using the white beam from a Ag X-ray tube employing an accelerating voltage of 40 kV and a current of 20 mA. A $TlGaSe_2$(001) wafer measuring 3 mm × 5 mm × 0.87 mm with evaporated Ti/Au contacts was placed in a Model eV-480 test fixture connected to a Model eV-550 preamplifier box. The bias voltage was 190 V, corresponding to an electric field of 2.375×10^5 V m^{-1}. The 5 mm × 5 mm × 5 mm CZT SPEAR detector was operated at a bias voltage of 1000 V, corresponding to an electric field of 2×10^5 V m^{-1}. For both the $TlGaSe_2$ and the commercial CZT detector, the signal was transferred to an Ortec amplifier (Model 572A) with a gain of 100 and shaping time of 0.5 μs before it was evaluated by a dual 16 K input multichannel analyzer (Model ASPEC-927) with a USB interface and subsequently read into the MAESTRO-32 software. A schematic of the setup is shown in the Supporting Information. The details of the photoconductivity experiments will be reported elsewhere.

Single-crystal XRD data were collected at 293 K on a STOE 2T image plate diffractometer with Mo Kα radiation (λ = 0.71073 Å). An analytical absorption correction was applied to the data using the program X-Red on an optimized shape obtained with the aid of X-Shape software. The structures were solved by direct methods and refined with the SHELXTL software package. Thermal displacement parameters were anisotropically refined for all atomic positions. Data were collected on several single crystals, to check for consistency in the lattice parameters.

Band structure calculations were carried out using the full-potential linearized augmented plane wave (FLAPW) method[22] with the screened-exchange local density approximation (sX-LDA).[23] The core and the valence states were treated fully and scalar relativistically, respectively. Experimental lattice parameters and atomic coordinates obtained in the single-crystal refinement reported below were used for the calculations. The energy cutoffs for the interstitial plane-wave basis and the star functions were 12.3 and 144 Ry, respectively.

RESULTS AND DISCUSSION

Synthesis and Crystal Growth. An example of a single-crystal of $TlGaSe_2$ grown with a modified Bridgman technique is shown in Figure 4A. Figure 5 shows the powder XRD pattern for ground crystals of the Bridgman-grown $TlGaSe_2$. The peak positions match the theoretical pattern from the reported crystal structure,[10,11] as well as that from the new single-crystal

refinement reported here, and thus confirm the single-phase nature of the Bridgman-grown crystal. Because of its layered structure, there is substantial preferred orientation of the sample. Hence, (00*l*) Bragg peaks are overly intense, whereas peaks with (*hkl*) normal to the [001] direction are partially extinct. No reaction is observed with the fused-silica crucible, provided that the starting materials are sufficiently pure. However, failure to remove impurities (e.g., an oxide film on a Ga shot) can result in silica attack. Since elemental thallium is very reactive and readily forms an oxide, it is advantageous to prereact it with selenium to form the congruently melting TlSe, which can be then purified through an initial Bridgman growth run. The top and bottom part of the grown TlSe ingot can be discarded to minimize impurities with segregation coefficients larger and smaller than unity, respectively. As a beneficial side effect, through the initial formation of TlSe, a highly exothermic reaction is avoided in the formation of $TlGaSe_2$. In the Bridgman-grown samples, single-crystalline domains were observed to grow parallel to the *ab* plane. Consequently, the crystals were cut perpendicular to the growth direction and then mechanically cleaved along the growth direction using a razor blade. The crystals show mirrorlike surfaces, and no mechanical polishing was deemed necessary prior to the electrical or optical measurements. Wafers with suitable dimensions were cut for X-ray and γ-ray detector purposes; e.g., the crystal shown on the right in Figure 4C measures ~5 mm × 8 mm × 1 mm. Crystals as large as ~10 mm × 5 mm × 2 mm were obtained. Because of the limited dimensions of the detector housing, cutting of larger specimens was not attempted. The attenuation length in $TlGaSe_2$ remains below 1 mm for energies up to ~130 keV (Figure 2), and, hence, the dimensions of these crystals imply efficient absorption for photon energies up into this energy range.

To measure photoconductivity and detector response, it is important to have single-crystalline specimens, because multiple crystal domains will potentially have different transport properties, leading to false peaks in the pulse height spectra.[2] The quality of the crystal wafers can be checked using transmitted polarized light, since misaligned domains will transmit at different angles when the sample is rotated perpendicular to the polarized light. Therefore, the transmission of polarized light provides a fast and facile way to ensure single crystallinity, exclude multiple-domain wafers, or gain information on how to cut the wafers to obtain single-crystalline specimens. X-ray Laue back-reflection experiments were carried out to confirm the single-crystalline nature of the samples and allow sample orientation. In Figure 4B, a Laue X-ray back-reflection pattern from a $TlGaSe_2$ (001) surface is seen (see the Supporting Information for an indexing of the diffraction spots). This is in good agreement with the expected cleavage plane from the single-crystal refinement, which shows layers in the *ab* plane of corner-sharing octahedra bonded via weak Tl−Se bonds.

Single-Crystal X-ray Diffraction and Stacking Faults. $TlGaSe_2$ crystallizes in the monoclinic $C2/c$ $KInS_2$ structure.[8,10,11] In the structure, each Ga atom is tetrahedrally coordinated to four Se atoms, which, in turn, are in octahedral coordination to two Ga and four Tl atoms. Corner-sharing $GaSe_4$ tetrahedra form $[Ga_4Se_{10}]$ adamantine clusters, which then share corners to create infinite $[GaSe_2]^-$ layers in the *ab* plane (Figure 1A). The $[GaSe_2]^-$ layers have grooves running along the *a*- and *b*-axes that are large enough to accommodate the Tl atoms to form slabs of $TlGaSe_2$ (Figure 1B). The slabs then stack along the *c*-axis (Figure 1C). Therefore, the Tl atoms (both Tl(1) and Tl(2)) are not located between the layers but actually are "buried" in the $[GaSe_2]^-$ layers. For this reason, distinct crystallographic planes can then act as cleavage planes for the crystals and cause stacking faults (to be discussed later).

The Tl atoms are six-coordinated to Se atoms, adopting a trigonal prismatic arrangement. Two of these bonds bridge between $[GaSe_2]^-$ layers. For Tl(1), these interlayer bonds (having bond lengths of 3.288(4) and 3.296(4) Å) are significantly shorter than those for Tl(2), which are 3.393(3) and 3.418(3) Å. Nevertheless, these are all long and weak bonds, which lead to easy cleaving of the crystals parallel to the *ab* plane. Because of the strong Ga−Se covalent bonding in the *ab* plane and weak Tl−Se interlayer bonding, the crystal structure suggests large anisotropy in the transport properties. Surprisingly, however, the present band structure calculations, as well as literature studies,[24] reveal little anisotropy with a large dispersion from both the valence band maximum and the conduction band minimum to the *X*, *Y*, and *Z* points of the Brillouin zone (discussion below). This is attributed to the significant degree of covalent character of Tl···Se bonding, supported by the present and literature band structure calculations,[24] which essentially electronically "cross-links" the layers to produce a more three-dimensional system. Weak interlayer bonds have been observed in $TlGaSe_2$ and the similar layered compound TlS using ^{203}Tl and ^{205}Tl NMR.[8,25,26] This is in contrast, for example, to the isostructural alkali-metal analog $KGaSe_2$ which features mainly ionic bonding perpendicular to the layers.

Previously, there has been speculation as to whether stacking faults contribute to activated charge transport behavior in materials with observed activation energies of 0.2−0.4 eV in resistivity studies.[12,19,20] Stacking faults have been observed in $TlGaSe_2$[27,28] and in the isostructural KMQ_2 systems (with M = Al, Ga, and Q = Se, Te),[29] and are generally common to 2D systems with weak interlayer bonding. In $TlGaSe_2$ and KMQ_2, the faults arise from small energetic differences in making small shifts along $\pm[110]$ and $\pm[1\bar{1}0]$.[27,29] In reciprocal space, McMorrow et al. found that these stacking faults lead to a smearing of the lattice points along c^*.[27] Comparison of the datasets on $TlGaSe_2$[27] and KMQ_2[29] reveal that the effect is much less pronounced in $TlGaSe_2$, compared to its alkali-metal counterparts. Again, this can be explained by the stronger interlayer bonding in $TlGaSe_2$ than in KMQ_2, because of the more-covalent nature of interaction of the Tl^+ ions, relative to the alkali-metal ions. Nevertheless, these stacking faults can act as traps and recombination sites, as observed in layered GaSe,[30] and will contribute to a decrease in carrier mobility.[30,31] No effects of stacking faults are visible in our crystallographic dataset; even so, stacking faults in such materials must be taken into account when studying the electronic properties.

Spectroscopy. In order to accurately probe the optical properties of $TlGaSe_2$ and check for possible defect or impurity states, we measured the transmittance, reflectance, and photoluminescence spectra of single crystals. From the reported literature, it is unclear what the magnitude of the band gap of $TlGaSe_2$ is and whether it is of a direct or indirect nature.[12,19,21,32,33] In order to clarify this point, measurements of the single-crystal transmittance (T) and reflectance (R) were conducted on a 126-μm-thick crystal isolated from the Bridgman-grown sample. From R and T, the absorption coefficient (α) can be determined.[34] In Figure 6, α is plotted as a function of incident photon energy. In the present setup and for the

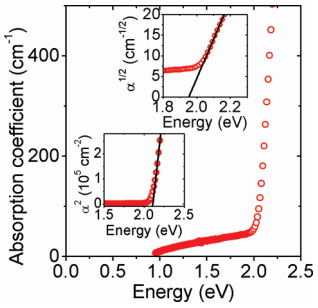

Figure 6. Absorption spectrum of a 126-μm-thick $TlGaSe_2$ crystal cleaved to expose the (001) surface. Insets shows linear fits to α^2 and $\alpha^{1/2}$.

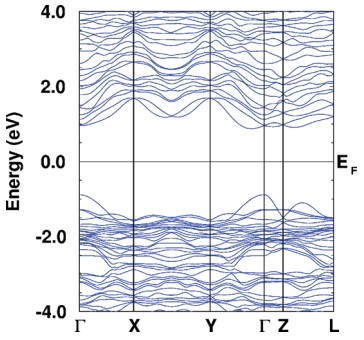

Figure 7. Electronic band structure of $TlGaSe_2$ calculated using the screened-exchange local density approximation (sX-LDA).

present sample thickness (d = 126 μm), it is not possible to reliably measure absorption coefficients above ~500 cm^{-1}. This is a highly underestimated value, because we were unable to prepare sufficiently thin samples to appreciably measure the absorption above the band gap. The electronic structure calculations on $TlGaSe_2$ and the direct nature of the transitions give a calculated theoretical absorption coefficient exceeding 1 000 000 cm^{-1}, a few electron volts above the band gap (not shown).

For indirect band gaps, a linear fit to $\alpha^{1/2}$ versus energy gives the indirect band gap as an intercept with the x-axis, whereas direct band gaps show a linear fit to α^2. Linear fits to the absorption coefficient data (Figure 6, insets) give 1.95 eV for the indirect band gap model and 2.11 eV for the direct band gap model. This is in agreement with previous absorption studies.[12,21] The direct and indirect band gaps are close in energy, as corroborated by the band structure calculations given below, which predict an indirect band gap of 1.76 eV separated by 0.09 eV from a direct gap. $TlGaSe_2$ is well-suited for X-ray and γ-ray detection, because the band gap is large enough to minimize thermally generated charge carriers, yet small enough to create large numbers of electron−hole pairs in the energy cascade following an absorbed photon, because of a low pair creation energy.[1−5,35]

Previously, deep states attributed to structural defects and impurities have been observed in $TlGaSe_2$ in studies of its optical[21] and electronic properties.[12,19,20,36] Provided these deep states also exist in the present samples, photoluminescence measurements can potentially determine the energy levels if these states lead to radiative recombination. In GaSe, photoluminescence bands in the forbidden gap, which increase

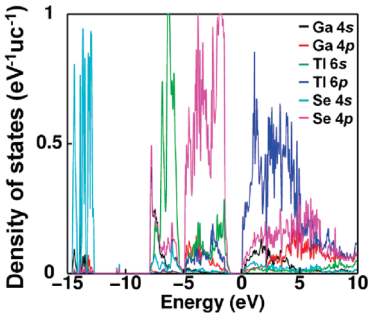

Figure 8. Element orbital contributions to the electronic density of states (per eV per unit cell), as a function of the energy relative to the Fermi level at 0 eV.

in intensity with the amount of structural defects,[37] have been attributed to stacking faults.[31,37] Consequently, we looked for photoluminescence from a $TlGaSe_2$ (001) wafer from room temperature down to 23 K, but no peaks were observed. Indirect-band-gap semiconductors are often inefficient photoluminescent materials, and the indirect band gap of $TlGaSe_2$ along with nonradiative recombination processes can explain the absence of PL peaks. Nevertheless, Gasanly et al. did observe rapid thermal quenching of the near-band-edge PL peak at 1.94 eV above 18 K,[32] which could explain the lack of PL in the present study, which was limited by our measurement setup to temperatures of 23 K and above.

Electronic Structure. In agreement with previous literature reports, the present band structure calculations for $TlGaSe_2$ show an indirect band gap (Figure 7).[24] We find that the valence band maximum is located at the Γ point of the Brillouin zone, while the conduction band minimum occurs along the Γ-Y direction. Kashida et al., on the other hand, found the conduction band minimum to be situated along the L-Z line. However, these authors did not include spin orbit coupling in their calculations,[24] which might be the cause of this discrepancy. Screened-exchange LDA shows an indirect band gap of 1.76 eV, which is in close agreement with the experimental band gap of 1.95 eV. The indirect gap is energetically separated by only 0.09 eV from a direct band gap at Γ.

The bottom of the conduction band is mainly composed of Tl 6p orbitals, whereas the top of the valence band is mostly due to Se 4p orbitals (see Figure 8). The delocalized nature of these orbitals results in valence and conduction bands with relatively large dispersion, which is favorable for the high charge carrier mobilities desired in detector materials. In agreement with the observation by Kashida et al.,[24] we find a considerable cross-band-gap interaction between the Tl 6p and Se 4p orbitals, which indicates significant covalent nature of the Tl−Se bonds in $TlGaSe_2$. The band structure in Figure 7 shows large dispersion near the band edges, especially near the valence band maximum. This suggests that the effective masses of the charge carriers are small, especially the hole carriers, which should result in good intrinsic properties for radiation detection.

Despite the promising theoretical results, knowledge of the true carrier effective masses in $TlGaSe_2$ will require more work, because there seems to be some controversy in the experimental literature. For example, optical measurements suggest small reduced effective masses of 0.2 m_0 cross-plane (0.15 m_0 in-plane) for the electron−hole pair.[21] However, Hall measurements

dx.doi.org/10.1021/cm200946y |*Chem. Mater.* 2011, 23, 3120–3128

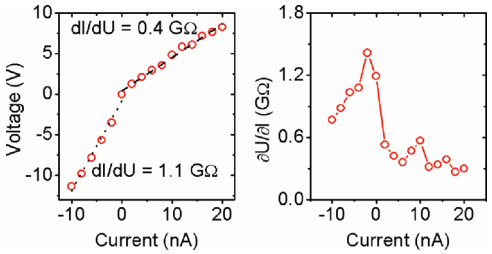

Figure 9. (A) Current−voltage ($I-V$) characteristics of a typical $TlGaSe_2$ wafer measured perpendicular to the *ab* plane. (B) Voltage derivative of the voltage shown in panel A, as a function of the current.

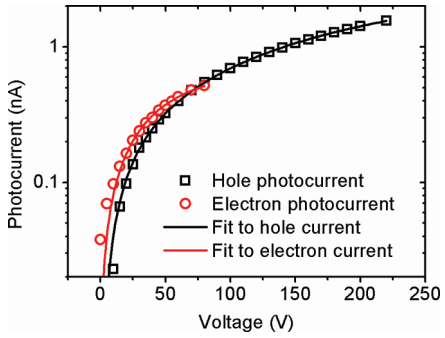

Figure 10. Hole photocurrents (shown in black) and electron photocurrents (shown in red) of a 0.87-mm-thick $TlGaSe_2$ wafer under forward and reverse bias, respectively.

show effective masses of $m_e = (0.33-0.37)m_0$ and $m_h = (0.52-0.68)m_0$.[20,36,38] Similarly, as mentioned above, NMR shows interlayer overlap, which can be explained by the observed dispersion along the valence band Γ−Z line.[8] In CdTe, the density of states effective masses are $0.11m_0$ and $0.73m_0$ for electrons and holes, respectively.[2] Since mobility scales linearly with the inverse of the effective mass, a high hole $\mu\tau$ product is not feasible in CZT. According to the present band structure calculations, $TlGaSe_2$ has no such intrinsic barrier to high $\mu\tau$ products for electrons or holes, which makes it attractive for further materials optimization.

Our theoretical analysis shows that band structure calculations using the sX-LDA method[23] can provide an accurate and insightful assessment of the electronic band structure and energy band gap.[39−44] In the present case, calculations reveal that $TlGaSe_2$ possesses promising properties, with a band gap energy and band dispersion appropriate for a detector material. Conversely, this also allows us to theoretically select and discard materials before we undertake labor-intensive crystal growth and characterization efforts.

Electrical and Photoelectrical Characterization. $TlGaSe_2$ is usually grown as a *p*-type conductor.[36,38,45] Photoconductivity and thermally activated behavior in the electrical resistivity have shown the existence of acceptor states 0.21−0.43 eV above the valence band.[12,19−21] These acceptor states are assigned to structural defects and impurities.[12,19,20,36] The room-temperature resistivities are highly anisotropic (up to $\rho_\perp/\rho_{||} = 10^5$), with in-plane resistivity values ($\rho_{||}$) of $2.7-2 \times 10^4$ Ω cm (see refs 19, 36, and 45) and cross-plane resistivities ($\rho_\perp$) of 10^4-10^{10} Ω cm.[8,19,20,45,46] Previous studies of the carrier mobilities showed values of 23−99 $cm^2\ V^{-1}\ s^{-1}$ for electrons[38,45] and 61−65 $cm^2\ V^{-1}\ s^{-1}$ for holes.[20,36,38,45] Improved crystal growth is likely to eliminate crystal defects and impurities, which, in turn, should increase the resistivity and mobility values. Higher mobilities and reported carrier lifetimes in the millisecond range[47] suggest that a high $\mu\tau$ product is feasible in $TlGaSe_2$. Combined with the wide indirect band gap of ∼1.8−2.0 eV,[12,19,21,33] $TlGaSe_2$ can be developed into an efficient detector material.

In order to avoid dark currents in the X-ray or γ-ray detector, it is important to maximize the resistivity of the material. High resistivities permit higher bias voltages and deeper depletion depths, hence higher drift velocities of the generated carriers. A minimum resistivity of $\sim 10^8-10^9$ Ω cm is generally recommended[2,3] for room-temperature operation, and detector-grade CZT has resistivities of $\sim 10^{11}$ Ω cm.[4] The current−voltage ($I-V$) characteristics of a 5 mm × 3 mm × 0.87 mm crystal measured perpendicular to the *ab* plane are shown in Figure 9A. The nonlinearity in the $I-V$ curve is evident, however; linear regions are observed above and below 0 V. This is attributed to Schottky barrier formation, because of differences in work functions of the contact material and the electron affinity of $TlGaSe_2$.[48] It is inherently difficult to make stable, high-quality contacts to materials with very high resisitivity,[3] and, in the present study, we did not observe ohmic contacts to $TlGaSe_2$. The nonlinearity is a common phenomenon with detector-grade materials and is also observed in CZT.[49] The derivative of the voltage, with respect to the current (Figure 9B), suggests that the resistance is in the gigaohm (GΩ) range and, based on the crystal dimensions, we estimate the resistivity to be in the 10^9 Ω cm range.

Important parameters for the assessment of X-ray and γ-ray detector materials are the $\mu\tau$ values of the two carrier types. The generated carriers must reach the electrodes in order to be measured. The diffusion length (λ) in the device is given by $\lambda = \mu\tau E$, where E is the electric field in the material. Hence, the detector energy resolution increases with increasing values of $\mu\tau$, because more carriers can reach the electrodes. In order to evaluate the $\mu\tau$ product for electrons and holes, we performed photoconductivity measurements on suitably sized $TlGaSe_2$ crystals using visible-light irradiation. Effects such as surface currents and surface recombination have a negative impact on detector performance.[48,50−53] For strongly absorbed light, the photoconductivity can be modeled and $\mu\tau$ values can be obtained using the following relation:[54]

$$I(U) = \frac{I_0 \mu\tau U}{L^2}\left[\frac{1-\exp\left(\frac{-L^2}{\mu\tau U}\right)}{1+\frac{L}{U}\left(\frac{s}{\mu}\right)}\right] \quad (1)$$

Here, I is the photocurrent, I_0 the saturation current, L the sample thickness, and U the applied voltage. In CZT, the $\mu\tau$ values obtained from our photoconductivity measurements are in good agreement with measurements using ionizing radiation,[55,56] which confirms the reliability of our $\mu\tau$ values. The surface recombination parameter s/μ reduces the charge collection efficiency and should be minimized to optimize detector performance. Both the $\mu\tau$ and s/μ values can be estimated from photoconductivity measurements. The wavelength of the incident laser light (633 nm) used in the photoconductivity setup is strongly absorbed, because the corresponding photon energy is larger than the band-gap energy. Consequently, photoconductivity measurements with

Table 1. Material Properties of the Presented $TlGaSe_2$ Crystal Obtained from Fits to the Photoconductivity, Optical Absorption, and $I-V$ Data

$\mu\tau_e$ ($cm^2\ V^{-1}$)	$(s/\mu)_e$ ($V\ cm^{-1}$)	$\mu\tau_h$ ($cm^2\ V^{-1}$)	$(s/\mu)_h$ ($V\ cm^{-1}$)	$E_{g,d}$ (eV)	$E_{g,i}$ (eV)	$\rho_\perp$ (Ω cm)
$6.0(6) \times 10^{-5}$	NA	$9.2(6) \times 10^{-6}$	97(7)	2.1(1)	1.95(2)	$\sim 10^9$

wavelengths above the band gap are particularly sensitive to surface recombination, because photon absorption occurs in the vicinity of the surface. The surface recombination parameter (s/μ) for the holes was $\sim$97 V cm^{-1}. Surface recombination is particularly strong for cut and polished wafers and less pronounced for cleaved surfaces. With suitable etchants, the s/μ value can be reduced considerably (e.g., exposing a polished CZT surface for 2 min to a 2% bromine in methanol solution can reduce the s/μ value from 173 V cm^{-1} to <10 V cm^{-1}).[49]

Figure 10 shows the electron (red) and hole (black) photoconductivities for $TlGaSe_2$. Fits to the data with eq 1 yield a value of $\mu\tau_h = 9.2(6) \times 10^{-6}$ $cm^2\ V^{-1}$ at an incident wavelength of 633 nm. A similar fit for negatively biased $TlGaSe_2$ gives a value of $\mu\tau_e = 6.0(6) \times 10^{-5}$ $cm^2\ V^{-1}$. (Details regarding material properties such as photoconductivity, optical absorption, and current–voltage ($I-V$) relations are given in Table 1.) The corresponding values for CZT are $\mu\tau_e \approx (0.4-11) \times 10^{-3}$ $cm^2\ V^{-1}$ and $\mu\tau_h \approx (0.3-9) \times 10^{-5}$ $cm^2\ V^{-1}$ (values from both photoconductivity and ionizing radiation measurement),[2,4] and it is seen that, for holes, $TlGaSe_2$ is approaching the values for CZT. The $\mu\tau_e/\mu\tau_h$ values for the $TlGaSe_2$ crystals are also comparable to those of other heavily investigated materials, such as HgI_2 and TlBr.[4] These results are very promising, and improved crystal growth with higher purity elements and subsequent zone refinement is likely to not only increase the resistivity of $TlGaSe_2$ but also enhance $\mu\tau$ values by reducing scattering centers such as impurities and native defects.

Detector Properties. Previous studies of X-ray or γ-ray detection using $TlGaSe_2$ have not been reported. However, radiation damage studies of γ-irradiation (Co-60 source with 1.17 MeV and 1.33 MeV radiation) found no structural changes in $TlGaSe_2$ upon large radiation doses (up to 200 MR) at high incident flux ($\sim$180 R/s), although changes were observed in the electronic transport properties.[57] This suggests that the $TlGaSe_2$ structure is fairly resistant to radiation.

To investigate whether hard X-rays are detectable by the $TlGaSe_2$ wafers, we performed white Ag X-ray irradiation experiments at room temperature. The pulse height spectrum obtained for a detector using a $TlGaSe_2$ crystal is shown in Figure 11 with the corresponding X-ray spectrum from a commercial CZT SPEAR detector, using a 5 mm × 5 mm × 5 mm CZT wafer (shown for comparison). The characteristic lines of Ag of 22.2 and 24.9 keV are not resolved in either the $TlGaSe_2$-based detector or the commercial CZT detector, but a convoluted peak for Ag Kα at $\sim$22 keV is observed in both cases.

The accelerating voltage of the X-ray tube was kept at 40 kV, yet counts are obtained at photon energies much higher than 40 keV for the $TlGaSe_2$ detector. This is because of a comparatively slow read-out time of the $TlGaSe_2$ detector, generally referred to as "pulse pileup",[58] which, in some cases, counts multiple photons within the time window of 0.25 μs used in the experiment. Thus, the lower $\mu\tau$ products found for $TlGaSe_2$ causes the full width at half maximum (fwhm) for the peak to be wider. Higher-quality crystal growth and wafer production with

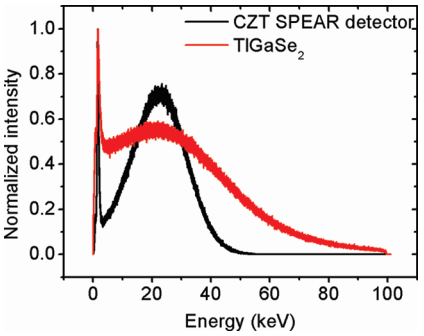

Figure 11. Detection of a white beam from a Ag X-ray tube, using a $TlGaSe_2$ wafer. A spectrum obtained from a commercial CZT detector (black line) is shown for comparison.

appropriate mechanical and chemical surface treatment are expected to produce crystals with lower defect densities and higher resistivities, which, in turn, will increase the $\mu\tau$ product and minimize dark currents. This should lead to $TlGaSe_2$-based detectors with smaller fwhm in the recorded pulse height spectrum. Similarly, stacking faults might be unavoidable in this material, because of the weak interlayer bonding; hence, it might be advantageous to alloy indium with gallium, as previously suggested,[15] or silver with thallium. This will create strain centers, which would help to pin gliding dislocations.[15] A beneficial side effect would be the increase in X-ray and γ-ray stopping power from the increase in average atomic number. $Tl_2GaInSe_4$ has been successfully synthesized in the literature and has an indirect band gap of 1.86 eV.[59] Crystals with in plane resistivities of $\rho_{||} = 2.7 \times 10^7$ Ω cm have been reported,[60] which is far above the $\rho_{||}$ range of $2.7-2 \times 10^4$ Ω cm reported for $TlGaSe_2$.[19,20,45] Similarly, the reported electron mobilities of 290 $cm^2\ V^{-1}\ s^{-1}$ in the plane[60] are also significantly higher than in $TlGaSe_2$.[38,45] These results suggest that In substitution can improve the electronic properties, possibly by eliminating gliding dislocation through the induced structural strain.

CONCLUSIONS

The present study has demonstrated the great potential of $TlGaSe_2$, which is a member of the class of thallium chalcogenides for X-ray and γ-ray detection. The current results for $TlGaSe_2$ show that band structure calculations have an important role to play in the identification of potential X-ray and γ-ray detector materials. Detailed information such as band gap energy, and the nature of the band structure and its dispersion, can now be obtained with the necessary accuracy. Large single-crystalline wafers of $TlGaSe_2$ can be cut and cleaved from Bridgman-grown samples. Improved crystal growth and better mechanical processing of the wafers with fewer impurities and reduced structural and strain defects are expected to produce crystals with higher resistivities, higher $\mu\tau$ products, and lower surface recombination (s/μ). No evidence of stacking faults was observed in the present single-crystal diffraction data set; however, their presence cannot be ruled out. Alloying of $TlGaSe_2$ with In on the Ga site or Ag on the Tl site might be a way to pin moving dislocations, thereby minimizing formation of faults. The relatively high mobility-lifetime $(\mu\tau)$ values obtained from photoconductivity measurements indicate $TlGaSe_2$ is attractive for further development for use in detector applications. The potential of $TlGaSe_2$ is indeed highlighted by the ability of these

dx.doi.org/10.1021/cm200946y |Chem. Mater. 2011, 23, 3120–3128

unoptimized crystalline wafers to detect and resolve Ag K radiation. $TlGaSe_2$ and its solid solutions hold great promise as X-ray and γ-ray detector materials, and the systems merit further study.

■ ASSOCIATED CONTENT

Supporting Information. The supporting information includes the following: Figure S1, which contains photographic details from the synthesis; Figure S2, which shows a schematic of the setup used in the photoconductivity measurements; Figure S3, which shows a schematic of the setup used in the measurement of X-ray detector properties; and Figure S4, which is a Laue back reflection photograph recorded on a $TlGaSe_2$(001) surface and oriented using the program OrientExpress. Also provided is Table S1, which shows details of the single-crystal structure refinement, and a CIF file of the single-crystal refinement. This material is available free of charge via the Internet at http://pubs.acs.org.

■ AUTHOR INFORMATION

Corresponding Author

*Tel.: 847-467-1541. Fax: 847-491-5937. E-mail: m-kanatzidis@northwestern.edu.

■ ACKNOWLEDGMENT

This work is supported by a Department of Homeland Security grant (No. ARI-MA: 2010-DN-077-ARI042-02). S.J. acknowledges the Danish Research Council for Nature and Universe for funding.

■ REFERENCES

(1) Milbrath, B. D.; Peurrung, A. J.; Bliss, M.; Weber, W. J. *J. Mater. Res.* **2008**, *23*, 2561–2581.
(2) Schlesinger, T. E.; Toney, J. E.; Yoon, H.; Lee, E. Y.; Brunett, B. A.; Franks, L.; James, R. B. *Mater. Sci. Eng., R* **2001**, *32*, 103–189.
(3) Owens, A.; Peacock, A. *Nucl. Instrum. Methods Phys. Res., Sect. A* **2004**, *531*, 18–37.
(4) Owens, A. *J. Synchrotron Rad.* **2006**, *13*, 143–150.
(5) McGregor, D. S.; Hermon, H. *Nucl. Instrum. Methods Phys. Res., Sect. A* **1997**, *395*, 101–124.
(6) Szeles, C. *Phys. Status Solidi B* **2004**, *241*, 783–790.
(7) Amman, M.; Lee, J. S.; Luke, P. N. *J. Appl. Phys.* **2002**, *92*, 3198–3206.
(8) Panich, A. M. *J. Phys.: Condens. Matter* **2008**, *20*, 293202.
(9) Acikgoz, M.; Kazan, S.; Mikailov, F. A. *Appl. Spectrosc. Rev.* **2009**, *44*, 181–209.
(10) Delgado, G. E.; Mora, A. J.; Perez, F. V.; Gonzalez, J. *Cryst. Res. Technol.* **2007**, *42*, 663–666.
(11) Henkel, W.; Hochheimer, H. D.; Carlone, C.; Werner, A.; Ves, S.; Vonschnering, H. G. *Phys. Rev. B* **1982**, *26*, 3211–3221.
(12) El-Nahass, M. M.; Sallam, M. M.; Rahman, S. A.; Ibrahim, E. M. *Solid State Sci.* **2006**, *8*, 488–499.
(13) Seltzer, S. M. *Radiat. Res.* **1993**, *136*, 147–170.
(14) Ekinci, N.; Gurol, A.; Durna, D.; Gurbulak, B. *Anal. Lett.* **2010**, *43*, 1999–2008.
(15) Knuteson, D. J.; Singh, N. B.; Kahler, D.; Wagner, B.; Berghmans, A.; McLaughlin, S.; Schwartz, K. In *Hard X-Ray, Gamma-Ray, and Neutron Detector Physics XI*, 1st ed.; James, R. B., Franks, L. A., Burger, A., Eds.; Proceedings of SPIE, Vol. 7449; SPIE: San Diego, CA, 2009; p 744918.
(16) Kahler, D.; Singh, N. B.; Knuteson, D. J.; Wagner, B.; Berghmans, A.; McLaughlin, S.; King, M.; Schwartz, K.; Suhre, D.; Gotlieb, M. *Nucl. Instrum. Methods Phys. Res., Sect. A* **2010**, DOI 10.1016/j.nima.2010.09.057.
(17) Morgant, G.; Legendre, B.; Maneglier-Lacordaire, S.; Souleau, C. *Ann. Chim.-Sci. Mater.* **1981**, *6*, 315–326.
(18) Laugier, J.; Filhol, A. *J. Appl. Crystallogr.* **1983**, *16*, 281–283.
(19) Hanias, M. P.; Anagnostopoulos, A. N.; Kambas, K.; Spyridelis, J. *Mater. Res. Bull.* **1992**, *27*, 25–38.
(20) Qasrawi, A. F.; Gasanly, N. M. *Mater. Res. Bull.* **2004**, *39*, 1353–1359.
(21) Kalomiros, J. A.; Kalkan, N.; Hanias, M.; Anagnostopoulos, A. N.; Kambas, K. *Solid State Commun.* **1995**, *96*, 601–607.
(22) Wimmer, E.; Krakauer, H.; Weinert, M.; Freeman, A. J. *Phys. Rev. B* **1981**, *24*, 864–875.
(23) Bylander, D. M.; Kleinman, L. *Phys. Rev. B* **1990**, *41*, 7868–7871.
(24) Kashida, S.; Yanadori, Y.; Otaki, Y.; Seki, Y.; Panich, A. M. *Phys. Status Solidi A* **2006**, *203*, 2666–2669.
(25) Panich, A. M. *Appl. Magn. Reson.* **2004**, *27*, 29–39.
(26) Panich, A. M.; Kashida, S. *J. Phys.: Condens. Matter* **2004**, *16*, 3071–3080.
(27) McMorrow, D. F.; Cowley, R. A.; Hatton, P. D.; Banys, J. *J. Phys.: Condens. Matter* **1990**, *2*, 3699–3712.
(28) Banis, J.; Brilingas, A.; Grigas, J.; Guseinov, G. *Fiz. Tverd. Tela* **1987**, *29*, 3324–3329.
(29) Kim, J.; Hughbanks, T. *J. Solid State Chem.* **2000**, *149*, 242–251.
(30) Manfredo, C; Murri, R.; Rizzo, A.; Galassin., S; Ruggiero, L. *Phys. Rev. B* **1974**, *10*, 3387–3393.
(31) Shigetomi, S.; Ikari, T.; Nishimura, N. *Phys. Status Solidi A* **2001**, *185*, 341–348.
(32) Gasanly, N. M.; Serpenguzel, A.; Aydinli, A.; Baten, S. M. A. *J. Lumin.* **2000**, *86*, 39–43.
(33) Bakhyshov, A. E.; Boules, S.; Faradzhov, F. E.; Mamedov, M. S.; Tagirov, V. I. *Phys. Status Solidi B* **1979**, *95*, K121–K125.
(34) Smith, R. A. *Semiconductors*; Cambridge University Press: Cambridge, U.K., 1959.
(35) Alig, R. C.; Bloom, S. *Phys. Rev. Lett.* **1975**, *35*, 1522–1525.
(36) Qasrawi, A. F.; Gasanly, N. M. *Semicond. Sci. Technol.* **2004**, *19*, 505–509.
(37) Capozzi, V.; Montagna, M. *Phys. Rev. B* **1989**, *40*, 3182–3190.
(38) Guseinov, G. D.; Abdullayev, G. B.; Bidzinova, S. M.; Seidov, F. M.; Ismailov, M. Z.; Pashayev, A. M. *Phys. Lett. A* **1970**, *33*, 421–422.
(39) Bera, T. K.; Jang, J. I.; Song, J. H.; Malliakas, C. D.; Freeman, A. J.; Ketterson, J. B.; Kanatzidis, M. G. *J. Am. Chem. Soc.* **2010**, *132*, 3484–3495.
(40) Bera, T. K.; Song, J. H.; Freeman, A. J.; Jang, J. I.; Ketterson, J. B.; Kanatzidis, M. G. *Angew. Chem., Int. Ed.* **2008**, *47*, 7828–7832.
(41) Biswas, K.; Zhang, Q. C.; Chung, I.; Song, J. H.; Androulakis, J.; Freeman, A. J.; Kanatzidis, M. G. *J. Am. Chem. Soc.* **2010**, *132*, 14760–14762.
(42) Chung, I.; Song, J. H.; Jang, J. I.; Freeman, A. J.; Ketterson, J. B.; Kanatzidis, M. G. *J. Am. Chem. Soc.* **2009**, *131*, 2647–2656.
(43) Tsamourtzi, K.; Song, J. H.; Bakas, T.; Freeman, A. J.; Trikalitis, P. N.; Kanatzidis, M. G. *Inorg. Chem.* **2008**, *47*, 11920–11929.
(44) Ye, L. H.; Hoang, K.; Freeman, A. J.; Mahanti, S. D.; He, J.; Tritt, T. M.; Kanatzidis, M. G. *Phys. Rev. B* **2008**, 77.
(45) Shaban, H. T. *Mater. Chem. Phys.* **2010**, *119*, 131–134.
(46) Madelung, O. *Semiconductors: Data Handbook*, 3rd ed.; Springer: Berlin, 2004.
(47) Ashraf, I. M.; Abdel-Rahman, M. M.; Badr, A. M. *J. Phys. D: Appl. Phys.* **2003**, *36*, 109–113.
(48) Prokesch, M.; Szeles, C. *J. Appl. Phys.* **2006**, *100*, 8.
(49) Burger, A.; Groza, M.; Cui, Y.; Hillman, D.; Brewer, E.; Bilikiss, A.; Wright, G. W.; Li, L.; Fu, F.; James, R. B. *J. Electron. Mater.* **2003**, *32*, 756–760.
(50) Wright, G.; Cui, Y.; Roy, U. N.; Barnett, C.; Reed, K.; Burger, A.; Lu, F.; Li, L.; James, R. B. *IEEE Trans. Nucl. Sci.* **2002**, *49*, 2521–2525.

(51) Ruzin, A.; Nemirovsky, Y. *Appl. Phys. Lett.* **1997**, *71*, 2214–2215.
(52) Burshtein, Z.; Akujieze, J. K.; Silberman, E. *J. Appl. Phys.* **1986**, *60*, 3182–3187.
(53) Cui, Y.; Wright, G.; Kolokolnikov, K.; Barnett, C.; Reed, K.; Roy, U. N.; Burger, A.; James, R. B. In *Hard X-Ray and Gamma-Ray Detector Physics III*; Proceedings of SPIE, Vol. 4507; James, R. B., Ed.; SPIE: Bellingham, WA, 2001; pp 12−22.
(54) Many, A. *J. Phys. Chem. Solids* **1965**, *26*, 575.
(55) Cui, Y.; Groza, M.; Wright, G. W.; Roy, U. N.; Burger, A.; Li, L.; Lu, F.; Black, M. A.; James, R. B. *J. Electron. Mater.* **2006**, *35*, 1267–1274.
(56) Zanichelli, M.; Pavesi, M.; Zappettini, A.; Marchini, L.; Auricchio, N.; Caroli, E.; Manfredi, M. *IEEE Trans. Nucl. Sci.* **2009**, *56*, 3591–3596.
(57) Sheleg, A. U.; Iodkovskaya, K. V.; Kurilovich, N. F. *Phys. Solid State* **1998**, *40*, 1208–1210.
(58) Kapoor, S. S.; Ramamurthy, V. S. *Nuclear Radiation Detectors*; New Age International Ltd.: New Delhi, India, 1986.
(59) Qasrawi, A. F.; Gasanly, N. M. *Phys. Scr.* **2007**, *76*, 249–252.
(60) Qasrawi, A. F.; Gasanly, N. M. *Philos. Mag.* **2008**, *88*, 2899–2906.